Twisting light with micro-spheres produced by ultrashort light pulses

Martynas Beresna,[1,*] Mindaugas Gecevičius,[1] Nadezhda M. Bulgakova,[2] and Peter G. Kazansky[1]

[1]*Optoelectronics Research Centre, University of Southampton, Southampton, SO17 1BJ, UK*
[2]*Institute of Thermophysics SB RAS, 1 Lavrentyev Ave., 630090 Novosibirsk, Russia*
**mxb@orc.soton.ac.uk*

Abstract: We propose a radial polarizer based on light refraction on a transparent isotropic sphere. We demonstrate theoretically and experimentally that the circularly polarized light impinging on the sphere produces double charged optical vortex. The method is applied to generate optical vortices on a small scale using hollow micro-spheres produced by femtosecond laser in fused silica.

OCIS codes: (240.0240) Optics at surfaces; (260.5430) Polarization.

References and links

1. A. Mair, A. Vaziri, G. Weihs, and A. Zeilinger, "Entanglement of the orbital angular momentum states of photons," Nature **412**(6844), 313–316 (2001).
2. G. Molina-Terriza, J. P. Torres, and L. Torner, "Management of the angular momentum of light: preparation of photons in multidimensional vector states of angular momentum," Phys. Rev. Lett. **88**(1), 013601 (2001).
3. E. Nagali, F. Sciarrino, F. De Martini, L. Marrucci, B. Piccirillo, E. Karimi, and E. Santamato, "Quantum information transfer from spin to orbital angular momentum of photons," Phys. Rev. Lett. **103**(1), 013601 (2009).
4. O. G. Rodríguez-Herrera, D. Lara, K. Y. Bliokh, E. A. Ostrovskaya, and C. Dainty, "Optical nanoprobing via spin-orbit interaction of light," Phys. Rev. Lett. **104**(25), 253601 (2010).
5. D. G. Grier, "A revolution in optical manipulation," Nature **424**(6950), 810–816 (2003).
6. J. E. Curtis and D. G. Grier, "Structure of optical vortices," Phys. Rev. Lett. **90**(13), 133901 (2003).
7. V. Y. Bazhenov, M. V. Vasnetsov, and M. S. Soskin, "Laser-beam with screw dislocations in their wave-fronts," JETP Lett. **52**, 429–431 (1990).
8. L. Allen, M. W. Beijersbergen, R. J. C. Spreeuw, and J. P. Woerdman, "Orbital angular momentum of light and the transformation of Laguerre-Gaussian laser modes," Phys. Rev. A **45**(11), 8185–8189 (1992).
9. M. W. Beijersbergen, R. P. C. Coerwinkel, M. Kristensen, and J. P. Woerdman, "Helical-wave-front laser-beams produced with a spiral waveplate," Opt. Commun. **112**(5-6), 321–327 (1994).
10. M. Beresna, P. G. Kazansky, Y. Svirko, M. Barkauskas, and R. Danielius, "High average power second harmonic generation in air," Appl. Phys. Lett. **95**(12), 121502 (2009).
11. E. Brasselet, N. Murazawa, H. Misawa, and S. Juodkazis, "Optical vortices from liquid crystal droplets," Phys. Rev. Lett. **103**(10), 103903 (2009).
12. L. Marrucci, C. Manzo, and D. Paparo, "Optical spin-to-orbital angular momentum conversion in inhomogeneous anisotropic media," Phys. Rev. Lett. **96**(16), 163905 (2006).
13. G. Biener, A. Niv, V. Kleiner, and E. Hasman, "Formation of helical beams by use of Pancharatnam-Berry phase optical elements," Opt. Lett. **27**(21), 1875–1877 (2002).
14. M. Beresna, M. Gecevicius, P. G. Kazansky, and T. Gertus, "Radially polarized optical vortex converter created by femtosecond nanostructuring of glass," Appl. Phys. Lett. **98**(20), 201101 (2011).
15. J. A. Ferrari, W. Dultz, H. Schmitzer, and E. Frins, "Achromatic wavefront forming with space-variant polarizers: Application to phase singularities and light focusing," Phys. Rev. A **76**(5), 053815 (2007).
16. R. Oldenbourg, "Analysis of edge birefringence," Biophys. J. **60**(3), 629–641 (1991).
17. S. Kanehira, J. H. Si, J. R. Qiu, K. Fujita, and K. Hirao, "Periodic nanovoid structures via femtosecond laser irradiation," Nano Lett. **5**(8), 1591–1595 (2005).
18. E. Toratani, M. Kamata, and M. Obara, "Self-fabrication of void array in fused silica by femtosecond laser processing," Appl. Phys. Lett. **87**(17), 171103 (2005).
19. J. Song, X. S. Wang, X. Hu, Y. Dai, J. R. Qiu, Y. Cheng, and Z. Z. Xu, "Formation mechanism of self-organized voids in dielectrics induced by tightly focused femtosecond laser pulses," Appl. Phys. Lett. **92**(9), 092904 (2008).
20. B. Poumellec, L. Sudrie, M. Franco, B. Prade, and A. Mysyrowicz, "Femtosecond laser irradiation stress induced in pure silica," Opt. Express **11**(9), 1070–1079 (2003).
21. E. N. Glezer and E. Mazur, "Ultrafast-laser driven micro-explosions in transparent materials," Appl. Phys. Lett. **71**(7), 882–884 (1997).

#147498 - $15.00 USD Received 13 May 2011; revised 29 Jun 2011; accepted 12 Jul 2011; published 15 Sep 2011

22. W. Watanabe and K. Itoh, "Motion of bubble in solid by femtosecond laser pulses," Opt. Express **10**(14), 603–608 (2002).
23. S. Juodkazis, K. Nishimura, S. Tanaka, H. Misawa, E. G. Gamaly, B. Luther-Davies, L. Hallo, P. Nicolai, and V. T. Tikhonchuk, "Laser-induced microexplosion confined in the bulk of a sapphire crystal: evidence of multimegabar pressures," Phys. Rev. Lett. **96**(16), 166101 (2006).
24. R. Graf, A. Fernandez, M. Dubov, H. J. Brueckner, B. N. Chichkov, and A. Apolonski, "Pearl-chain waveguides written at megahertz repetition rate," Appl. Phys. B **87**(1), 21–27 (2007).
25. Y. Bellouard and M.-O. Hongler, "Femtosecond-laser generation of self-organized bubble patterns in fused silica," Opt. Express **19**(7), 6807–6821 (2011).
26. J. P. Vigouroux, J. P. Duraud, A. Le Moel, C. Le Gressus, and D. L. Griscom, "Electron trapping in amorphous SiO_2 studied by charge buildup under electron bombardment," J. Appl. Phys. **57**(12), 5139–5144 (1985).
27. P. Martin, S. Guizard, Ph. Daguzan, G. Petite, P. D'Oliveira, P. Meynadier, and M. Perdrix, "Subpicosecond study of carrier trapping dynamics in wide-band-gap crystals," Phys. Rev. B **55**(9), 5799–5810 (1997).
28. Y. D. Glinka, S.-H. Lin, L.-P. Hwang, Y.-T. Chen, and N. H. Tolk, "Size effect in self-trapped exciton photoluminescence from SiO_2-based nanoscale materials," Phys. Rev. B **64**(8), 085421 (2001).
29. N. O. Young, J. S. Goldstein, and M. J. Block, "The motion of bubbles in a vertical temperature gradient," J. Fluid Mech. **6**(03), 350–356 (1959).
30. S. C. Hardy, "The motion of bubbles in a vertical temperature gradient," J. Colloid Interface Sci. **69**(1), 157–162 (1979).
31. P. Török, "Imaging of small birefringent objects by polarised light conventional and confocal microscopes," Opt. Commun. **181**(1-3), 7–18 (2000).
32. E. Brasselet, M. Malinauskas, A. Zukauskas, and S. Juodkazis, "Photopolymerized microscopic vortex beam generators: Precise delivery of optical orbital angular momentum," Appl. Phys. Lett. **97**(21), 211108 (2010).

1. Introduction

A property of light beams to carry angular momentum has attracted considerable attention due to numerous applications ranging from quantum optics [1–3] to microscopy [4] and micromanipulation [5, 6]. Orbital angular momentum (OAM) is found in light beams with phase singularities which possess a nonzero azimuthal energy flow. Commonly used methods for generating beams with OAM are based on the exchange of orbital angular momentum with matter [7–9]. Recently an efficient coupling of angular momentum carried by circularly polarized light with OAM was demonstrated in systems with the radial symmetry: second harmonic generation in laser induced plasma [10], liquid crystal droplets [11] and radially variant birefringent waveplates [12–14]. Additionally, it was shown that radial polarizer can introduce orbital angular momentum into the beam [15]. The advantage of this type process is that the helicity of the output wave front can be controlled by the handedness of incident light polarization. However, such systems could not be straightforwardly downsized, preventing from widespread application in integrated optics. A system which could provide desirable compact form and possess radial symmetry is a bubble or a void (we distinguish these two structures by the presence or absence of a filler gas respectively). If voids or bubbles embedded in glass have a relatively high refractive index contrast, they exhibit edge birefringence [16] related to differential transmission of *s* and *p*-polarizations.

In this paper, we propose and demonstrate a radial polarizer based on an isotropic transparent sphere. As a result of angular momentum conservation, spherical interface leads to optical vortex generation which is directly observed on microscopic spherical voids produced inside the glass by femtosecond laser. A fundamental explanation for controllable laser-induced formation of such voids with reduced refractive index is also provided. We anticipate that the observed type of angular momentum interaction localized in several microns and sensitive to the handedness of circular polarization will open new opportunities in quantum optics, optical trapping, and manipulation.

2. Theory

Let us consider a circularly polarized light incident on an interface of two media with different refractive indices n_1 and n_2. As a result of differential transmission, transmitted light is elliptically polarized with major axis directed perpendicular to the interface and can be analyzed as superposition of linear E_{linear} and circular $E_{circular}$ polarizations (Fig. 1):

$$E_{ref} = \left(t_p(\theta) - t_s(\theta)\right) \cdot E_{linear} + t_s(\theta) \cdot E_{circular}, \quad (1)$$

#147498 - $15.00 USD Received 13 May 2011; revised 29 Jun 2011; accepted 12 Jul 2011; published 15 Sep 2011

where t_p, t_s are the Fresnel transmission coefficients for p and s polarized light and θ is the angle of incidence. In the explicit form one can write:

$$t_p(\theta) - t_s(\theta) = \frac{2\left(\frac{n_1^2}{n_2^2} - 1\right) a(\theta)\cos\theta}{\frac{n_1}{n_2}\left(\cos^2\theta + a^2(\theta)\right) + \left(\frac{n_1^2}{n_2^2} + 1\right) a(\theta)\cos\theta}, \tag{2}$$

where

$$a(\theta) = \sqrt{1 - \left(\frac{n_1}{n_2}\sin\theta\right)^2}.$$

Due to a high degree of symmetry, a sphere adds an azimuthal angle as an additional degree of freedom. Thus, for interfaces of spherical shape the transmitted and reflected light will be partially polarized (see Eq. (1) correspondingly in radial and azimuthal directions.

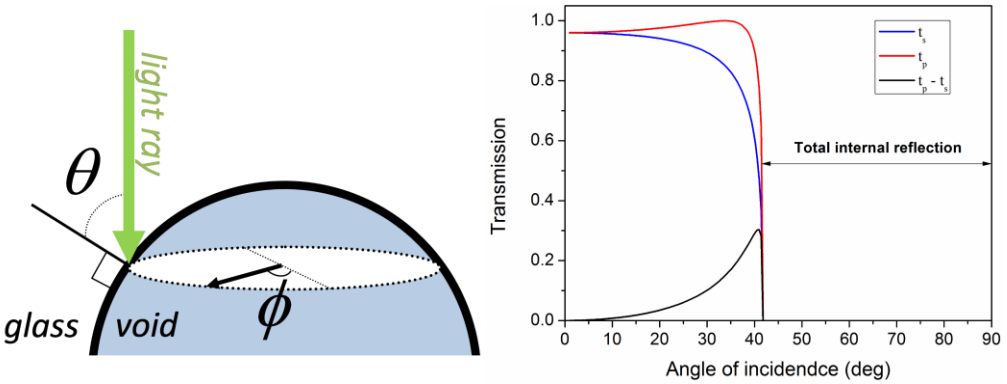

Fig. 1. (Left) Schematic representation of light ray impinging a void embedded in glass. (Right) Transmission at the glass/air interface for s and p polarized light versus angle of incidence θ. The black curve represents differential transmission, which in the case of incident circular polarization produces partially linear (p) polarization.

As in the Rayleigh range the light wave front is flat, the polarizing effect of the spherical shape can be approximated as a radial polarizer and described by the following Jones matrix:

$$M = \begin{pmatrix} \cos^2\phi & \cos\phi\sin\phi \\ \cos\phi\sin\phi & \sin^2\phi \end{pmatrix}, \tag{3}$$

where ϕ is the polar angle. After refraction E_{linear} (the incident field is left circularly polarized, $\underline{E}_{in} = E_0 \times [1, i]$) can be written as:

$$E_{linear} = M \cdot E_{in} = \frac{1}{2} E_0 e^{i2\phi} \begin{pmatrix} 1 \\ -i \end{pmatrix} + \frac{1}{2} E_0 \begin{pmatrix} 1 \\ i \end{pmatrix}. \tag{4}$$

Hence, the incident beam after passing the radial polarizer splits into two circularly polarized waves of opposite handedness. The wave, which retains incident polarization state, has a plane wave front. However, the other one acquires an explicit $\exp(i2\phi)$ phase factor, indicating the presence of a phase singularity and associated OAM $l = 2\hbar$. As a result, the beam transforms into a circularly polarized optical vortex as it is confirmed by our modeling based on the Jones matrix formalism (Fig. 2). Right-hand circularly polarized beam after passing through the sphere will acquire OAM $l = -2\hbar$. Therefore, the input polarization determines the sign of the output OAM. Superposition of two circularly polarized waves, to

#147498 - $15.00 USD Received 13 May 2011; revised 29 Jun 2011; accepted 12 Jul 2011; published 15 Sep 2011

which the incident beam splits, yields a vortex with radial distribution of electrical field polarization and non-zero intensity in the center. The optical vortex and plane wave can be separated by a combination a quarter-wave plate and linear polarizer, which serve as a circular polarizer.

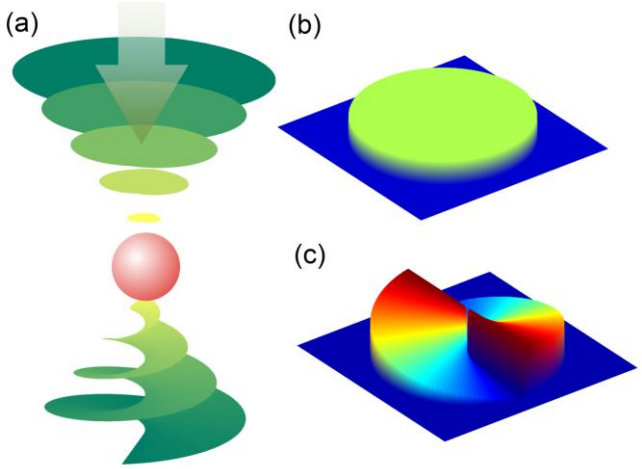

Fig. 2. (a) Optical vortex generation on an isotropic sphere. Incident circularly polarized light with plane front (l = 0) after refraction on a spherical surface is partially converted into an optical vortex with the orbital angular momentum l = 2ħ. (b, c) Wave-front profiles of incident and transmitted electric field modelled using the Jones matrix formalism.

3. Experiment details

To demonstrate this optical phenomenon, we created localized structural changes in silica glass using a tightly focused femtosecond laser beam. The experiments were carried out with a regeneratively amplified mode-locked Yb:KGW (Yb-doped potassium gadolinium tungstate) laser delivering 270 fs pulses with 200 kHz repetition rate and 6 W average power at 1030 nm wavelength. The energy of the pulse could be varied by a combination of an achromatic half-wave plate and a Glan polarizer.

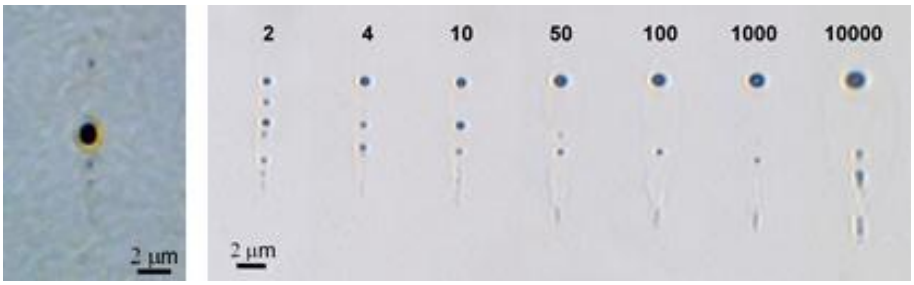

Fig. 3. (Left) Glass modification after single pulses (enhanced contrast). (Right) Cross-sections of femtosecond laser-induced structures. The number of pulses is indicated above. The laser beam is entering from the top.

The average laser power used in the experiments was 325 mW. The laser beam was focused about 60 µm below the surface of silica glass plate via a 100× (NA = 0.7) microscope objective. The sample was mounted on three-axial air-bearing motorized stages. Polarization state was controlled with achromatic quarter-wave plates inserted before the objective to avoid a potential polarization distortion due to reflection from the mirrors.

A series of dots was written by electronically controlling the laser output via a built-in pulse picker, while laterally translating the sample (Fig. 3). The exposure time per single dot

#147498 - $15.00 USD Received 13 May 2011; revised 29 Jun 2011; accepted 12 Jul 2011; published 15 Sep 2011

was in the range from 4 μs to 20 s. In order to avoid form birefringence induced by linear polarization, we used circular polarization.

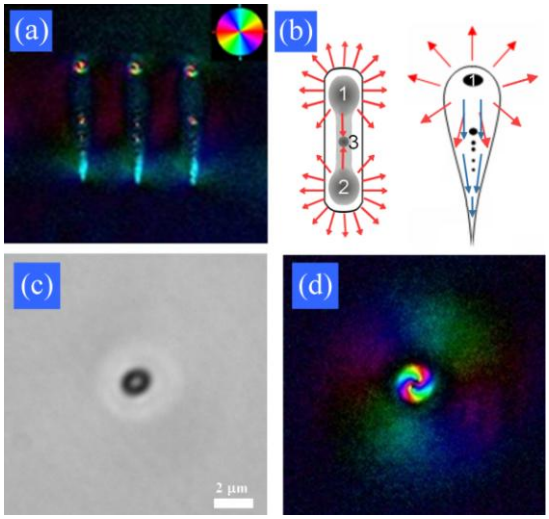

Fig. 4. a) Abrio image represented in pseudo colour showing direction of the slow axis (see inset), of the structure formed by femtosecond laser in silica glass (exposition 0.01 s). b) Corresponding schematic of the heat-affected regions created by single (left) and multi-pulse (right) irradiation. Red arrows indicate stress directions and blue ones show stressed material flow inducing compaction. Note that for single pulses the temperature is nearly-uniform along the quasi-cylindrical region axis while the stress distribution is dumbbell shaped (shown in grey). Tensile failure at the hot region ends leads to the consecutive chain rupture between the points 1 and 2 with creation of one or several voids 3. c) Top view of the same structure (a) with corresponding Abrio image (d).

After laser writing, the cross-sections of laser induced structures were investigated with a transmission optical microscope and a quantitative birefringence measurement system Abrio (CRi Inc.). Under our experimental conditions, we observed the formation of self-aligned spherical voids (Fig. 3) whose origin is still under discussion [17–19]. In contrast with previous results [18] we observed void formation even after single pulse irradiation (Fig. 3, left). In dots written with only several pulses, the voids were evenly distributed along the light propagation direction. At longer expositions (≥50 pulses per dot) smaller voids were erased leaving only single voids in the head and central part of the structures. The diameter of the induced voids varied from 600 nm to 2 μm depending on the exposure time. The analysis of birefringence revealed relatively strong anisotropy induced in the structure tail (Fig. 4a) while from the top of the structure radially symmetric stress could be observed (Fig. 4d). Additionally, "scissors effect" [20] could be observed outside the irradiated volume. In the front and central parts, where material was softer and, as a result, evenly distributed, no stress related birefringence was observed under all examined writing conditions.

4. Void formation dynamics

In fact, internal cavity (a bubble or a void) formation in transparent materials at ultrashort irradiation regimes is a complicated multiphysics phenomenon resulting from generation of localized dense plasmas whose recombination brings matter into a highly stressed state. The geometry of the heat-affected region and the matter state in this region (softened, molten, or ionized vapor) depend on the irradiation parameters among which the focusing geometry plays an important role. A lot of efforts have been made for understanding formation of internal cavities in glass materials (see, e.g., [21–25]). Depending on the irradiation conditions, the formation of cavities is attributed to different scenarios from spontaneous bubble nucleation in the molten phase [25] to the 10 TPa pressures induced by tight focusing of laser beams [23]. A detailed description of the void formation dynamics in our particular

#147498 - $15.00 USD Received 13 May 2011; revised 29 Jun 2011; accepted 12 Jul 2011; published 15 Sep 2011

experiments is now under progress, which includes the Maxwell equations for modeling the laser energy absorption with determining the heat-affected region and the thermoelastoplastic model based on the finite element method to follow the evolution of stress fields within irradiated matter. Here we shortly outline how the void formation dynamics emerges from the preliminary theoretical analysis, thus pointing up an intermediate scenario between those reported in [23] and [25].

During a single laser pulse, dense electron plasma is generated via the multi-photon ionization and avalanche processes in an elongated prefocal region of a quasi-cylindrical shape with rounded bases (Fig. 4b). Typical sizes of the laser-heated regions are ≥10 μm in length and ≤1 μm in diameter. As electron recombination in fused silica occurs via a trapping-like process with characteristic time of ~150 fs, in 1 ps after pulse action the excited region is heated to the temperatures ≥2000 K and brought to a highly stressed state. The stress maxima (stress concentrators) in excess of 10 GPa are located at the butt-ends of the long narrow laser-heated zone where material is melted/softened. These stress maxima are conditioned by the hot material expansion facilitated along the softened "channel". As the stress level is more than two orders of magnitude greater as compared to the tensile strength (~50 MPa) and exceeds the yield stress (~4.5 GPa) of cold fused silica (note that with heating these mechanical parameters considerably decrease), material rupture happens in the stress maxima locations with creation of void structures. Sudden material rupture with creation of voids at the hot region ends generates emission of the unloading waves and relocation of the maximum stress sites toward the center of the hot structure where again the tensile strength can be exceeded. Depending on the temperature (and, hence, stress) level, a third void can be created in app. a half-way between the voids 1 and 2 (Fig. 4 b) or a chain rupture occurs with formation of several successive voids along the laser-excited region. However, even slight variations of the temperature along the hot region axis and associated variations of material strength can influence locations and sizes of interstitial voids.

Due to defect creation upon electron recombining (self-trapped excitons and *E'* centers with lifetime up to ~1 ms [26–28]) and their preferential re-excitation, compared to the valence electrons, upon irradiation [27], each subsequent pulse generates a denser plasma (and, hence, higher temperature) in the front part of the structure around the void 1 (Fig. 4b) while a smaller portion of the laser energy is transferred to the structure tail. As a result, the heat-affected region transforms from a quasi-cylinder to a teardrop shape under multi-pulse irradiation. The hot matter is pressed out preferably to the structure tail (blue arrows) penning the voids located there and creating material compaction. On the contrary, the front void (indicated as '1' on the right-hand side in Fig. 4b) increases due to heat accumulation in the surrounding zone and migrates in the direction to the laser driven by difference in surface tension, developed by the temperature gradient between the front and back poles of the void [29,30].

5. Polarization conversion measurements

For the observation of optical vortex formation, a light emerging from a halogen lamp was circularly polarized and filtered with the bandpass filter (a central wavelength of 531 nm and a bandwidth of 30 nm) (Fig. 5). The sample was illuminated with a long working distance condenser set to 0.1 NA to ensure diffraction of the beam on the void. The light, transmitted through the sample, was collected with high NA objectives (0.9 and 0.6), passed through a quarter-wave plate and a linear polarizer filtering out background light, and projected on a digital CCD camera.

#147498 - $15.00 USD Received 13 May 2011; revised 29 Jun 2011; accepted 12 Jul 2011; published 15 Sep 2011

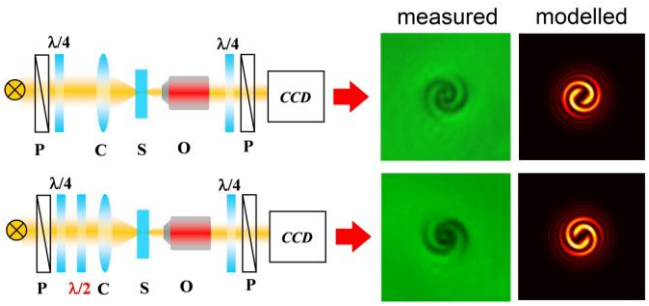

Fig. 5. Optical setups for optical vortex observation. P – polarizer, C – condenser, S – sample, O – objective. Vortex patterns (measured and modeled), observed under left and right handed polarizations, show mirror symmetry indicating reverse of orbital momentum sign.

When the void observed in circularly polarized light was slightly defocused (~10-20 μm), a distinctive two-branched spiral feature appeared which grew in size with increasing defocus (Fig. 5). Depending on positive or negative defocus was added, spiral changed its handedness. The spirals could be better seen in the focal plane located after the void. This asymmetry can be related to residual spherical aberrations which arise due to the mismatch of refractive indices at the void interior/fused silica interface. If the handedness of incident circular polarization was reversed by adding a half-wave plate, the spiral also changed its direction (Fig. 5). This clearly demonstrates that the spiral direction is defined by the incident circular polarization, as predicted by the modeling of the described optical system assuming a radial polarizer instead of a void. For comparison, using the Jones matrix formalism, we modeled the described optical system. The modeled patterns (see Fig. 5) are in good agreement with the measurements, confirming validity of the model and explanation of the phenomena given above. Identical chiral features were found in the structures produced under the same experimental conditions with a Ti:Sapphire laser (λ = 800 nm, τ_{pulse} = 150 fs) confirming that the observed spirals are the result of geometry of the modification.

In order to distinguish between stress and boundary related anisotropies, we inspected the bubble defects formed during glass preparation which presumably do not possess any stress birefringence. Similar two-branched spirals were observed for bubbles with diameter of 2-3 μm. Larger bubbles, however, did not produce such patterns. Such size dependence suggests that conversion efficiency is related to the ratio between the incident light beam spot size and the bubble diameter. Similar spiral shapes were predicted theoretically by modelling the behaviour of a Rayleigh scatterer in polarization microscope [31]. However, their origin was not clearly explained. We suppose that the spiral pattern is formed due to the superposition of left and right handed circular polarizations emerging when light couples with the bubble [32]. The presence of two branches clearly indicates that the OAM of the transmitted beam is $l = \pm 2\hbar$. This interference is also observed with the Abrio system and can be mistaken for a birefringent structure having whirlpool shape anisotropy. This ambiguity can be resolved by comparing images taken with left and right handed circular polarizations. The real birefringence, in contrast to the observed effect, is independent on the handedness of the circular polarization. Additionally, this suggests that the used microscope system can be effectively applied for characterizing phase singularities created by scattering or refraction on small particles.

In contrast to a conventional radial polarizer, the polarization efficiency of a void depends on the position (and, hence, angle) on the surface where light ray crosses the interface (see Eq. (1). The strongest effect is expected where the surface normal constitutes the Brewster angle with incident light (Fig. 1), i.e. where the differential transmission is the strongest. The total polarization conversion efficiency can be estimated by integrating ($t_p(\theta)$-$t_s(\theta)$) through all θ values, i.e. from 0 to 90 degree. Assuming that the refractive indices of the glass sample and a void are respectively 1.5 and 1, the conversion efficiency of circular polarization into optical vortex is about 2% and it largely depends on the refractive index contrast and angle of

#147498 - $15.00 USD Received 13 May 2011; revised 29 Jun 2011; accepted 12 Jul 2011; published 15 Sep 2011

incidence. One can expect that, for a ring-shaped incident beam (e.g. formed using axicon) impinging on the ring shaped area on the sphere, where the rays of light impinge at the Brewster angle and, hence, polarization effect is strongest, the conversion efficiency will increase to ~15%. Higher refractive index contrast would allow achieving efficiencies up to 40%. Alternatively, optical vortex can be generated in reflection. However, management of diverging light in reflection is challenging and requires a more complicated setup. Despite the low conversion efficiencies, the proposed optical vortex formation scheme is extremely simple and compact as opposed to conventional methods. Additionally, as it is related only to the geometry of voids, the described properties are universal and can be expected in countless situations.

Formation of optical vortices during femtosecond laser irradiation implies that, for circular polarization, partial angular orbital momentum interaction can occur in a multi-shot regime. The OAM acquired by the beam can interact with free electrons creating plasma whirlpools and lead to a new kind of laser-matter interaction. The flexibility of ultrafast laser direct writing also allows producing arrays of voids, which could be integrated in microfluidics systems for the handling of micro-objects (Fig. 6). Additionally, the resolution beyond the diffraction limit can be achieved with a circularly polarized vortex.

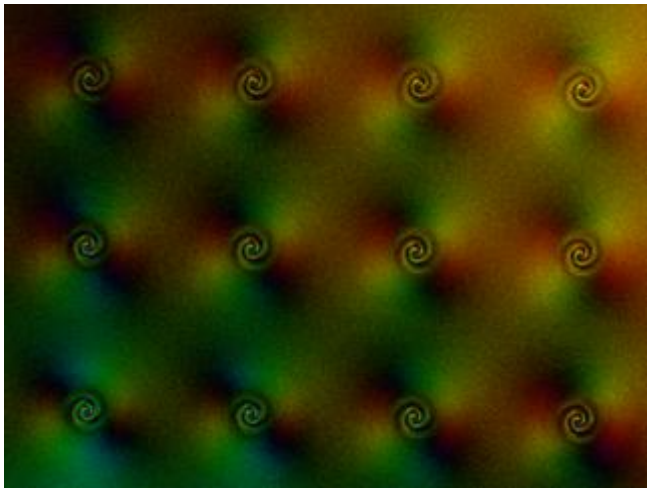

Fig. 6. Multiple vortex conversion with an array of micro-voids (period 10 μm).

6. Conclusions

In conclusion, we have proposed a radial polarizer based on an isotropic transparent sphere. We have identified and experimentally demonstrated the orbital angular momentum formation on isotropic micro-voids embedded in isotropic medium; the magnitude of OAM is determined by radial geometry of voids. The effect was successfully demonstrated on self-organized void arrays induced by tightly focused ultrashort pulses. This technique offers a practical alternative to conventional radial polarizers and a flexible way to produce dense arrays of optical vortex generators which could be used for integrated quantum optics and optofluidics.

Acknowledgement

The authors acknowledge insightful discussions with Rudolf Oldenbourg. The work was supported by the Engineering and Physical Sciences Research Council (EPSRC Project No. EP/E034802/1) and the project FEMTOPRINT, financed by the European Commission Factories of the Future program (FP7/ NMP/Project No 260103), http://www.femtoprint.eu/.

#147498 - $15.00 USD Received 13 May 2011; revised 29 Jun 2011; accepted 12 Jul 2011; published 15 Sep 2011